Development 124, 1301-1311 (1997)
Printed in Great Britain © The Company of Biologists Limited 1997
DEV3600

Loss of *cerebum* function ventralizes the zebrafish embryo

Shannon Fisher[1,*], Sharon L. Amacher[2] and Marnie E. Halpern[1]

[1]Department of Embryology, Carnegie Institution of Washington, 115 W. University Parkway, Baltimore, MD 21210, USA
[2]Institute of Neuroscience, University of Oregon, Eugene, OR 97403, USA

*Author for correspondence (e-mail: fisher@mail1.ciwemb.edu)

SUMMARY

Recent studies implicate ventrally derived signals, in addition to dorsal ones emanating from the organizer, in patterning the vertebrate gastrula. We have identified five overlapping deficiencies that uncover the zebrafish *cerebum* locus and dramatically alter dorsal-ventral polarity at gastrulation. Consistent with the properties of experimentally ventralized amphibian embryos, *cerebum* mutants exhibit reduced neurectodermal gene expression domains and an increase in derivatives of ventral mesoderm. Structures derived from paraxial and lateral mesoderm also are reduced; however, dorsal axial mesodermal derivatives, such as the hatching gland and notochord, are largely spared. The pleiotropic action of *cerebum* deficiencies, and the differential response of affected tissues, suggest that the *cerebum* gene may normally function as an inhibitor of ventralizing signals, a function previously ascribed to Noggin and Chordin in *Xenopus*. Analysis of the *cerebum* phenotype provides genetic evidence for the existence of ventralizing signals in the zebrafish gastrula and for antagonists of those signals.

Key words: gastrulation, mesoderm, organizer, *cerebum*, zebrafish

INTRODUCTION

In their experiments on the mechanisms of vertebrate gastrulation, Mangold and Spemann demonstrated the ability of cells from the amphibian dorsal blastopore lip to induce an ectopic embryonic axis upon transplantation to the ventral side of another embryo (Spemann and Mangold, 1924). The transplanted dorsal tissue was termed the organizer because of its ability to induce surrounding ventral host cells to develop as dorsal mesoderm and neurectoderm. The response of the embryo to the organizer is graded, with the amount of dorsal mesoderm and neurectoderm induced in proportion to the amount of organizer tissue present (Stewart and Gerhart, 1990). The organizer appears to be a conserved feature of vertebrate development, as embryonic regions with similar inductive properties have been demonstrated for zebrafish, chicken and mouse embryos (Kintner and Dodd, 1991; Ho, 1992; Storey et al., 1992; Beddington, 1994; Shih and Fraser, 1996).

The organizer is thought to produce extracellular signaling molecules responsible for its patterning influence on adjacent mesoderm and ectoderm, and, in the absence of these signals, cells assume ventral fates (refer to Slack, 1994). Candidates for such substances include Chordin and Noggin, both of which are expressed by the *Xenopus* organizer and have the ability to dorsalize mesoderm and to induce neurectoderm in animal cap assays (Sasai et al., 1994; Smith and Harland, 1992).

More recently, the model of an actively dorsalizing organizer and a ventral default state was challenged by the discovery that several bone morphogenetic proteins (BMPs), members of the TGFβ superfamily of growth factors, act as ventralizing factors that can override the influence of the organizer. Overexpression of BMP-4 or BMP-2 promotes development of ventral mesoderm and epidermis at the expense of dorsal mesoderm and neurectoderm (Jones et al., 1992; Fainsod et al., 1994; Clement et al., 1995; Hemmati-Brivanlou and Thomsen, 1995; Schmidt et al., 1995; Wilson and Hemmati-Brivanlou, 1995). Conversely, the development of dorsal mesoderm and neural tissue is promoted by reducing the activity of BMP-4, either through injections of antisense RNA (Steinbeisser et al., 1995), ectopic expression of a truncated receptor (Graff et al., 1994; Schmidt, et al., 1995) or expression of a non-cleavable BMP-4 (Hawley et al., 1995).

A connection between BMP signaling and the organizer-derived factors Noggin (Smith and Harland, 1992) and Chordin (Sasai et al., 1994) has come from the recent demonstration that both proteins directly bind BMP-4 and prevent it from binding its receptor (Piccolo et al., 1996; Zimmerman et al., 1996). Thus, it is likely that the dorsal patterning activity of the organizer in part arises from its ability to antagonize the activity of BMP-4 or other similar ventralizing factors. This interaction represents a highly conserved mechanism; *bmp-4* is a vertebrate homologue of the *Drosophila* gene *decapentaplegic* (*dpp*), required for proper dorsal-ventral patterning, and *dpp* is antagonized by *short gastrulation* (*sog*), the *Drosophila* homologue of *chordin*. Although no *Drosophila* homologue has been identified for *noggin*, *Xenopus noggin* RNA is capable of antagonizing *dpp* in *Drosophila* embryos (Holley et al., 1996). Analysis of mouse mutants produced by targeted gene disruption of *Bmp-4*, in which formation of mesoderm is substantially disrupted (Winnier et al., 1995), also provides genetic evidence for the importance of BMP-4 in early patterning of vertebrate embryos.

Studies of dorsal-ventral patterning in *Xenopus* have revealed a complex series of interactions, involving factors both maternally supplied and zygotically expressed, some having similar activities in misexpression assays (refer to Sive, 1993). Some genes have been identified that are thought to act upstream or downstream of BMP-4 signaling (Christian and Moon, 1993; Gawantka et al., 1995; Ladher et al., 1996; Schmidt et al., 1996). However, not all of the implicated genes have been easily placed in regulatory networks, nor have all of the genes involved been identified.

The zebrafish provides the means for exploring dorsal-ventral specification and its importance in vertebrate gastrulation using a genetic approach. Mutagenesis screens for early embryonic phenotypes (Kimmel, 1989; Mullins et al., 1994; Solnica-Krezel et al., 1994) have already identified genes proven to be important in the development of other vertebrates (Halpern et al., 1993; Schulte-Merker et al., 1994b; Talbot et al., 1995), demonstrating that genetic pathways are likely to be conserved. Furthermore, characterization of zebrafish mutations affecting dorsal-ventral patterning will not only facilitate studies on the interactions among known genes, but will reveal previously unidentified components of signaling pathways.

During a mutagenesis screen for early embryonic phenotypes, we identified *cerebum* (*crm*) mutants that exhibit defects in the morphogenesis and differentiation of mesodermal and ectodermal derivatives. As initial steps toward molecular identification of *crm*, we have mapped 5 gamma (γ)-ray-induced deficiencies to zebrafish linkage group 15 (LG 15) and we have ordered DNA markers in the *crm* chromosomal region. Analysis of the early phenotype of *crm* mutants suggests that the primary defect lies in dorsal-ventral specification at gastrulation, when ventral mesoderm and ectoderm are expanded at the expense of lateral mesoderm and neurectoderm. The *crm* loss-of-function phenotype reveals the existence of ventralizing signals in the zebrafish gastrula and provides genetic evidence for antagonists of those signals.

MATERIALS AND METHODS

Care and maintenance of fish lines

Techniques for the care and breeding of zebrafish were followed that have been previously described in detail (refer to Westerfield, 1993). The *cerebum* deficiency alleles (b305, b386, b409, c4, c47) are maintained as intercross lines or as outcrosses to wild-type (WT) fish of the Oregon AB background (provided by C. Walker and C. B. Kimmel). Each generation, heterozygous adults were identified by mating. In later experiments, carriers of *crm* deficiencies b386 and b409 were crossed to homozygotes for the dominant mutation *jaguar* (*jag*), which produces distinct body pigment patterns in heterozygotes and homozygotes (T. Mason and S. L. Johnson, personal communication) and, as described below, maps to the same chromosome arm as *crm*. Doubly heterozygous progeny (*crm*$^+$*; jag*$^-$/*crm*$^-$*; jag*$^+$) were maintained as interbreeding stocks. In these stocks, the *jag*$^-$/*jag*$^+$ heterozygotes, identified by their disrupted body pigment stripes and lack of tail pigment stripes, were always found to be *crm*$^-$/*crm*$^+$ and were readily identified from their sibling *jag*$^-$; *crm*$^+$ homozygotes.

Embryo culture and staging

Embryos were collected from natural matings and maintained in embryo medium (15 mM NaCl, 0.5 mM KCl, 1 mM $CaCl_2$, 1 mM $MgSO_4$, 0.15 mM KH_2PO_4, 0.05 mM Na_2HPO_4, 0.7 mM $NaHCO_3$) at 28.5°C. Embryos were staged according to standard morphological criteria (Kimmel et al., 1995).

γ-ray mutagenesis

γ-mutagenized stocks were generated essentially as described (Chakrabarti et al., 1983; Westerfield, 1993). Sperm was collected from WT (AB) males and pooled in ice-cold Hank's solution. A dose of 250-300 rads was delivered from a ^{137}Cs source and the sperm used to fertilize WT eggs expelled by squeezing of WT females.

Genetic mapping

To map the *crm* locus, we followed techniques developed by Postlethwait et al. (1994) that were used to produce a linkage map for the zebrafish based on random amplified polymorphic DNA (RAPD) markers in two partially inbred strains, AB and Darjeeling (DAR). A map cross panel of DNA was obtained by mating a b305/+ carrier with the AB background to a DAR fish. Haploid embryos were derived from the resultant F_1 AB/DAR *crm*$^-$/*crm*$^+$ females by fertilizing their eggs in vitro with UV-irradiated sperm (Streisinger et al., 1981). Genomic DNA was prepared from individual mutant and WT haploid embryos as described (Postlethwait et al., 1994). Typically, 0.2% of a sample was used in an individual polymerase chain reaction (PCR). Since the original mutagenesis was performed on AB fish, closely linked AB-specific RAPD markers only appeared in *crm* mutants, while closely linked DAR-specific markers were only present in WT haploids.

To detect RAPD markers by PCR, 25 μl reactions were set up in 96-well plates. The final reaction mix contained 10 mM Tris-HCl, pH 8.3, 1.5 mM $MgCl_2$, 50 mM KCl, 0.01% gelatin, 1 mg/ml BSA, 1 mM each dNTP, and 25 ng of the 10-base primer. Primers were purchased from Operon Technologies (San Diego, CA), as part of their standard 10-mer kits, and their primer designations are used in naming mapped RAPD markers. Reactions were taken through 37 cycles of 5 seconds at 94°C, 55 seconds at 92°C, 60 seconds at 36°C, 105 seconds at 72°C, followed by 7 minutes at 72°C. Pools of *crm* mutant and WT genomic DNA were screened by PCR for the approximately 400 previously mapped RAPD markers (Postlethwait et al., 1994), and comparisons were made of mutant and WT amplification products upon gel electrophoresis. Segregation of markers with the *crm* mutant phenotype was confirmed by retesting of individual haploids.

Recently, another mapping panel of zebrafish DNA was constructed based on simple sequence length polymorphism (SSLP) markers (Knapik et al., 1996, and E. W. Knapik, personal communication), and is being correlated with the original RAPD-based linkage map (J. Postlethwait and S. Horne, personal communication). SSLP markers were detected by PCR of individual haploid or diploid DNA samples, with 100 nM each of forward and reverse primers, purchased from Research Genetics (Huntsville, AL). Amplifications were performed as described (Knapik et al., 1996), with the omission of [γ^{32}P]ATP. Products were resolved by 5% Metaphor (FMC Bioproducts, Rockland, ME) agarose gel electrophoresis.

To amplify the 3′-UTR of *lim-1*, 25 μl reactions were set up as above with 500 ng of forward and reverse primers (provided by R. Toyama and I. Dawid). Reactions were taken through 30 cycles of 1 minute at 94°C, 1 minute at 50°C and 2 minutes at 72°C.

Conversion of N15 RAPD marker to sequence tagged site

RAPD primers typically amplify several bands, each of which is potentially an independently segregating marker. To make PCR primers specific for the LG15 15N.875 band, a sample of genomic DNA was amplified with the N15 RAPD primer and electrophoresed in low melting point agarose (FMC Bioproducts, Rockland, ME). The 875 bp band was excised and ligated in the pCR™II vector, using the TA Cloning Kit (Invitrogen). After DNA sequencing, primers were made to the ends of the fragment and used in amplifications with an annealing temperature of 55°C. The primer sequences are GTT-

TAACCCTTTAACAGG (forward) and TCAGTCATGCAGAATGGA (reverse), and the converted RAPD marker is referred to as 15N.875*.

RNA in situ hybridization

Digoxigenin-labeled antisense RNA probes were synthesized from linearized DNA templates using T3 [*krox-20* (Oxtoby and Jowett, 1993), *α-collagen II* (Yan et al., 1995)] or T7 [*lim5* (Toyama et al., 1995a), *lim1* (Toyama et al., 1995b) *otx1* and *otx2* (Li et al., 1994) *islet1* (Korzh et al., 1993), *goosecoid* (Thisse et al., 1994), *no tail* (Schulte-Merker et al., 1992), *eve1* (Joly et al., 1993)] RNA polymerase (Boehringer Mannheim). The *gata2* RNA probe (Detrich et al., 1995) was provided by Len Zon and Steve Pratt. Whole-mount in situ hybridizations were performed essentially as described (Thisse et al., 1993), using homozygous crm^{b305} or crm^{c4} mutant embryos. For in situ hybridizations on embryos prior to tail bud stage, before mutants can be sorted by morphology, embryos from intercrosses of crm^{c4}/crm^{+} carriers were used. Abnormal patterns of expression were present in the expected 25% of embryos. In some cases, following in situ hybridization and probe visualization, embryos were genotyped by DNA extraction and PCR amplifcation of the 15N.875* marker, which is absent in crm^{c4} homozygotes (data not shown).

Analysis of cell death

To detect cell death in mutant embryos and WT siblings, solutions and terminal transferase provided in the Apoptag Kit-Peroxidase (Oncor, Inc.) were used. Embryos were fixed and dehydrated as for in situ hybridization. After rehydration, they were incubated 1 hour at room temperature in equilibration buffer, then in working strength terminal transferase at 37°C for 2 hours. After several washes in stop/wash buffer, embryos were incubated with anti-digoxigenin antibody conjugated to alkaline phospatase (Boehringer Mannheim) and visualized as for RNA in situ hybridization.

RESULTS

Recovery of *cerebum* mutant alleles

In a mutagenesis screen for early embryonic phenotypes, *cerebum* mutants (crm^{b305}) were identified due to their dramatically reduced brains and eyes, and abnormal accumulation of cells caudal to the anus. During subsequent mutagenesis screens, three more γ-ray-induced mutations, b386, b409 and c47, were isolated by the remarkably similar phenotypes they produced. These were later confirmed to be allelic by failure to complement crm^{b305}. An additional allele, c4, was discovered by screening for non-complementation of the *crm* mutant phenotype in matings of b305/+ heterozygotes to progeny of γ-irradiated sperm.

With the exception of b409 (see Fig. 3C,F), all the *crm* alleles produced indistinguishable phenotypes as haploids (b305, b386, and c47), as homozygous diploids (b305, b386, and c4; Fig. 1B), or as transheterozygotes. The mutant phenotype was morphologically apparent during segmentation stages, when the tailbud was noticeably enlarged and the anterior neural keel shallower than in WT siblings (Fig. 1C,D). The observed frequency of *crm* mutant progeny from intercrosses of heterozygous fish, or in haploids produced from heterozygous females, indicated that the c4 allele segregates with simple Mendelian ratios (Table 1). In the case of crm^{b305} and crm^{b386}, we observed a lower frequency of *crm* mutants in haploid clutches and in intercross progeny of heterozygous carriers (Table 1). In addition, there was a second distinct cosegregating mutant phenotype present in both the haploid and diploid siblings of b305 and b386 mutants. These data suggest that each of these alleles results from a balanced reciprocal translocation. Additional evidence for this has come from genetic mapping studies.

Mapping of *crm* deficiencies to LG 15

The *crm* locus was placed on the zebrafish genetic map using PCR techniques that allow the identification of polymorphic DNA markers that segregate with a given mutant phenotype (Postlethwait et al., 1994). From the examination of 400 previously mapped random amplified polymorphic DNA (RAPD) markers, the linkage group (LG) 15 marker 9AB.930 was found to segregate with WT haploid siblings of crm^{b305} haploid mutants (data not shown). Subsequently the more distal marker

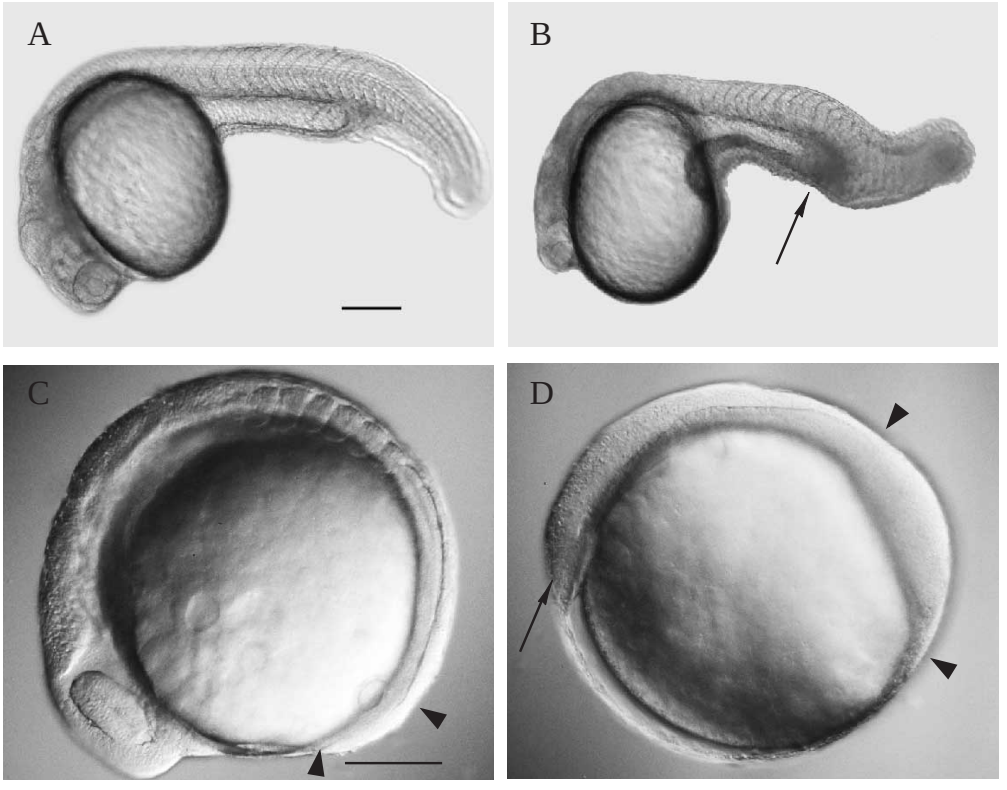

Fig. 1. Pleiotropic action of *cerebum* deficiencies on zebrafish development. (A) WT diploid pharyngula and (B) crm^{c4} mutant sibling at the 26 somite stage. The *crm* mutant is characterized by a reduced brain and eyes, and an abnormal accumulation of cells caudal to the anus (arrow). (C) WT embryo and (D) crm^{c4} sibling at the 8 somite stage. The mutant exhibits a shorter axis, a shallower anterior neural keel (arrow), and an enlarged tailbud (arrowheads). Scale bars, 200 μm.

Table 1. Segregation of *crm* mutant alleles

	Total no. of embryos	Observed no. (%) of *crm* mutants	Expected % mutants	No. (%) with other phenotype
b305 haploids	891	214(24%)	25%	*147(16%)
b386 haploids	83	15(12%)	25%	*16(19%)
b305/+ intercross	1233	35(2.8%)	6.25%	*35(2.8%)
b386/+ intercross	453	12(2.6%)	6.25%	*25(5.5%)
c4/+ intercross	769	199(26%)	25%	no

Haploids were derived from crm^{-}/crm^{+} females of the indicated alleles, as described in the Materials and Methods. Intercross progeny resulted from matings of crm^{-}/crm^{+} heterozygous fish. The predicted % of mutants is calculated from Mendelian frequencies for deletions (c4) and reciprocal translocations (b305, b386).

*In both b305/+ and b386/+ haploids and intercrosses, an additional, accompanying mutant phenotype was always observed: an early embryonic lethal termed *ghost*; and a dominant neural degeneration phenotype, respectively.

15N.875* was discovered to be deleted in genomic DNA of crm^{b305} haploids (Fig. 2A). A size polymorphism in 15N.875*, present in some WT fish (AB), demonstrated that haploid embryos displaying the distinct, early embryonic lethal phenotype (*ghost*) that accompanies crm^{b305} have the expected duplication of the LG 15 region that is deleted in *crm* mutants (Fig. 2A). Thus, mapping analysis supports the segregation data (Table 1), suggesting that crm^{b305} is maintained as a balanced reciprocal translocation.

DNA isolated from diploid or haploid mutant embryos was tested for the presence of additional LG 15 RAPD and simple sequence length polymorphism (SSLP) markers, and the data were used to generate a comparative map of the *crm* alleles (Fig. 2C). Mapping results indicated that all *crm* alleles are deficiencies, deleting variable extents of LG 15. This analysis has also allowed us to order SSLP markers. The absence of Z24 and the presence of Z5393 in c4 indicate that Z5393 is distal to Z24 on the LG 15 map. Finally, the presence of markers Z732 and Z1195 in b409 has allowed us to narrow the LG 15 region responsible for the *crm* phenotype to approximately 17 cM.

Mapping of *crm* deficiencies has revealed useful information about neighboring loci. The dominant viable pigmentation mutation *jaguar* (*jag*), which produces distinct heterozygous and homozygous phenotypes, had been previously mapped to LG 15 proximal to *crm* (Johnson et al., 1996). From evidence that *jag* maps near or distal to the breakpoints in b409 and b386 (see Fig. 1D), we predicted that recombination would be suppressed at the *jag* locus in carriers of these deficiencies. This was confirmed and has made it possible to maintain interbreeding stocks with the b386 and b409 alleles, without mating fish to identify *crm*/+ carriers, as described in Materials and Methods.

The homeodomain gene *lim-1* was also recently mapped to LG 15 (J. Postlethwait, personal communication), proximal to *jag*. We find that the *lim1* gene is disrupted in crm^{b409} (Fig. 2B), potentially causing the more severe brain phenotype of b409 homozygous mutants (see below).

Patterning is retained in the reduced *crm* mutant central nervous system

The *crm* deficiencies lead to a decreased development of the anterior central nervous system (CNS), obvious by morphology (Fig. 3A,B). An enhancement of this phenotype was observed in homozygous mutants bearing the crm^{b409} allele, which completely fail to develop recognizable forebrain, midbrain or eyes (Fig. 3C). In confirmation of the morphological defects, *krox-20* hindbrain expression is present (data not shown), but the diencephalic expression of *lim5* is absent in b409 homozygotes (Fig. 3F). This is in contrast to b305 homozygotes, in which the anterior domain of *lim5* expression is largely intact despite the decreased size of the brain (Fig. 3E).

To further characterize the CNS defects associated with the *crm* mutant phenotype, we examined regionally localized patterns of gene expression by whole-mount in situ hybridization. An early marker of hindbrain rhombomeres 3 and 5, *krox-20*, is first expressed at the end of gastrulation in a broad band of cells constituting presumptive rhombomere 3 and, later, is also expressed in rhombomere 5 (Oxtoby and Jowett, 1993). The rhombomere-specific domains of *krox-20* expression were present in the *crm* mutant hindbrain, although they were less intense and more variable in width than in WT (Fig. 3G,H). The homeodomain gene, *lim5*, a marker for the diencephalon (Toyama et al., 1995a), had a normal anterior limit of expression in *crm* mutants (Fig. 3D,E), as did the general forebrain marker *otx1* (Li et al., 1994) (Fig. 3I,J); however, both genes were expressed in reduced domains. Thus, anterior-posterior patterning of the crm^{-} brain is retained, although there is a pronounced reduction in cell number.

The *islet 1* (*isl1*) gene is a marker for subsets of identified neurons (Thor et al., 1991) and an indicator of dorsal-ventral polarity in the spinal cord. In zebrafish embryos, *isl1* is normally expressed in dorsal Rohon-Beard sensory neurons and in a subset of ventral primary motor neurons (Korzh et al., 1993; Inoue et al., 1994; Appel et al., 1995). In the *crm* mutant spinal cord, *isl1*-expressing cells corresponding to the dorsal Rohon-Beard cells and to the ventral motor neurons were present (Fig. 3K,L); however, the number of motor neurons per spinal cord segment was more variable compared to WT, with fewer *isl1*-expressing cells overall. The ventral midline cells of the spinal cord, the floor plate, were also present in *crm* mutants (see Fig. 4D). Differentiation of floor plate, motor neurons and dorsal sensory neurons suggests that dorsal-ventral patterning is largely preserved in the *crm* mutant spinal cord.

In summary, the CNS defects of crm^{-} embryos can be best characterized as a general decrease in cell number, with anterior structures most severely affected; however, anterior-posterior and dorsal-ventral patterning of the nervous system is largely intact.

To learn how early the CNS phenotype was apparent, we examined expression of neurectodermal markers at gastrulation. For example, *otx2*, a marker for the presumptive forebrain and eyes (Li et al., 1994) showed a decreased expression domain in *crm* mutants at gastrulation [80% epiboly] (Fig. 3M,N). In WT gastrulae, the *goosecoid* (*gsc*) gene is first expressed in the involuting prechordal mesoderm and, later, an additional domain of expression arises in the overlying neurectoderm (Thisse et al., 1994). Mesodermal *gsc* expression was intact in *crm* mutants but the neurectodermal component was greatly reduced (Fig. 3O-R). Expression of these two early markers of neurectoderm suggests that the overall reduction in size of the crm^{-} brain stems from a reduced number of neurectodermal cells at gastrulation.

One possible explanation is that the decrease in neurectoderm observed in *crm*$^{-}$ gastrulae results from increased cell death. Although morphologically we could not observe an overabundance of dying cells, we used a more sensitive whole-mount terminal transferase assay to directly visualize apoptotic cells in *crm*^{c4} mutants. In progeny from *crm*^{c4}/+ intercrosses, there was no noticeable increase in cell death during gastrulation or during early segmentation stages when *crm*^{c4} mutants could be readily distinguished from their WT siblings (data not shown). In contrast to the mutant CNS, by midsegmentation there was a pronounced increase in apoptotic cells in the *crm*$^{-}$ ventral tail (Fig. 3S,T). Thus, an increase in cell death in the neurectoderm is not the underlying cause of the reduced *crm*$^{-}$ nervous system. Instead, mis-specification during gastrulation could account for the reduction in neurectoderm.

A range of mesodermal defects in *crm*$^{-}$ embryos

In addition to their marked CNS defects, *crm*$^{-}$ embryos develop smaller somites and an accumulation of cells in the tail. To determine the extent to which mesodermal derivatives are

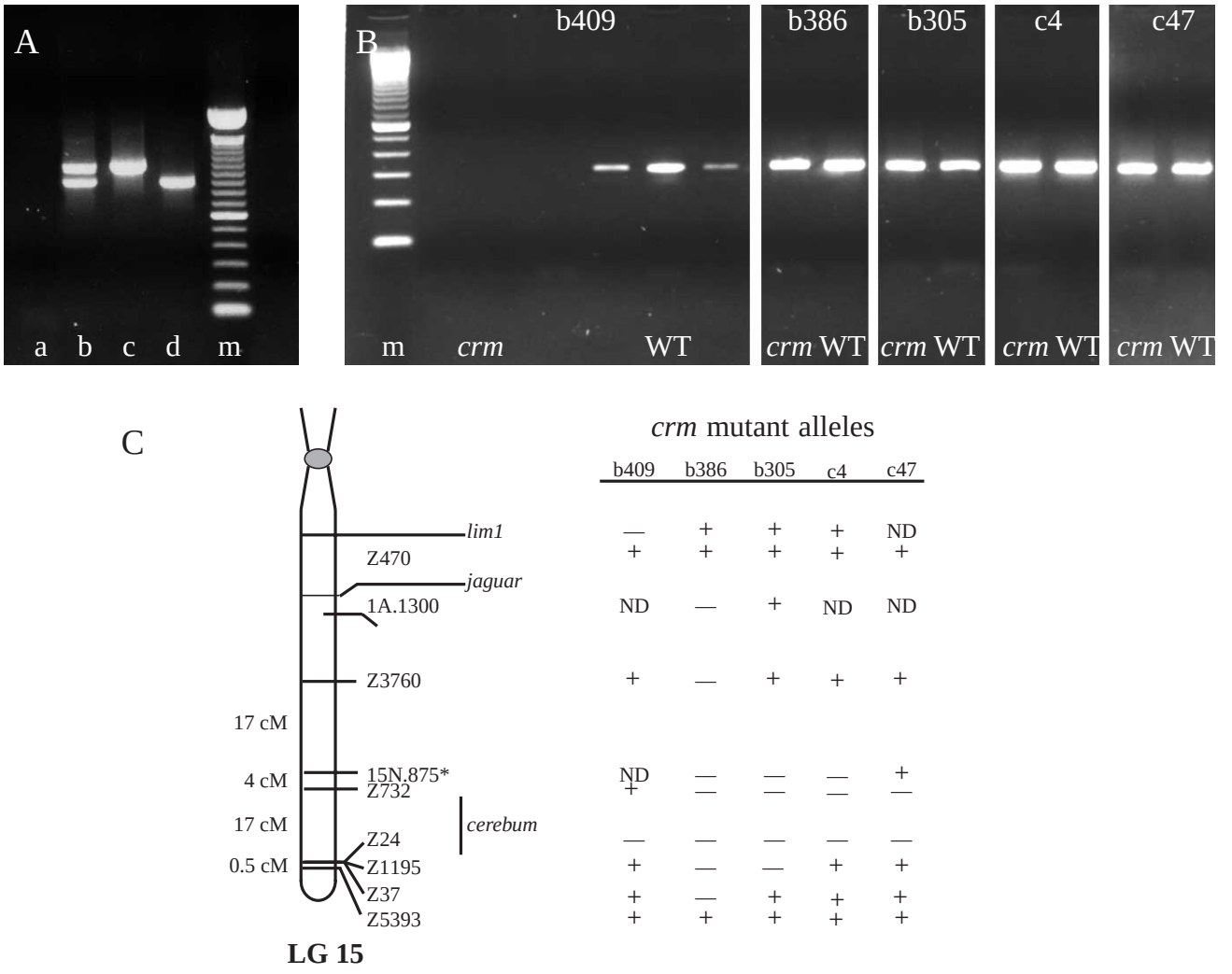

Fig. 2. Genetics and mapping of *cerebum* deficiency alleles. (A) The LG 15 marker 15N.875* is absent in PCR amplification of *crm*^{b305} haploid genomic DNA (lane a). In WT fish with the AB background, there is a size polymorphism of 15N.875*. In DNA from individual WT haploid siblings either the 1100 or 875 bp product was amplified by PCR (lanes c,d). Both size fragments were amplified from DNA of single haploid *ghost* embryos, the distinct embryonic lethal phenotype always accompanying *crm*$^{-}$ in the b305 allele (lane b). This suggests that *ghost* mutants have a LG 15 duplication corresponding to the translocated region containing *crm*$^{+}$. (B) Primers specific for the 3′-untranslated region of the *lim1* gene did not amplify the expected 320 bp product from DNA of *crm*^{b409} haploids. Consistent with this, in situ hybridization of b409 homozygotes failed to reveal any expression of *lim1* (S. Fisher, unpublished data). The expected *lim1* PCR product amplifies, however, from DNA of WT siblings, as well as from b386, b305, c4 and c47 *crm* mutants and their corresponding WT siblings. In A and B, m indicates the marker lane (100 bp ladder, Gibco-BRL). (C) Using PCR, *crm* mutant alleles were tested for the presence of LG 15 RAPD and SSLP (Z designation) markers (reference cross group 25, Knapik et al., 1996), as described in Materials and Methods. Genomic DNA samples from haploid mutants [b305, b386, b409 and c47] or homozygous diploids [c4] were tested; ND indicates that the presence (+) or absence (–) of a given marker has not yet been determined for that allele. The placement of Z470 relative to *lim1* and *jag* has not been precisely determined. Map distances, indicated to the left, represent a composite of data from the Postlethwait (Postlethwait et al., 1994; Johnson et al., 1996), Fishman and Driever (Knapik et al., 1996, and personal communication), and Halpern (unpublished data) laboratories. Analysis of the *crm* alleles demonstrates that they are overlapping deficiencies, and delimits the interval within which the *crm* locus resides to 17 cM.

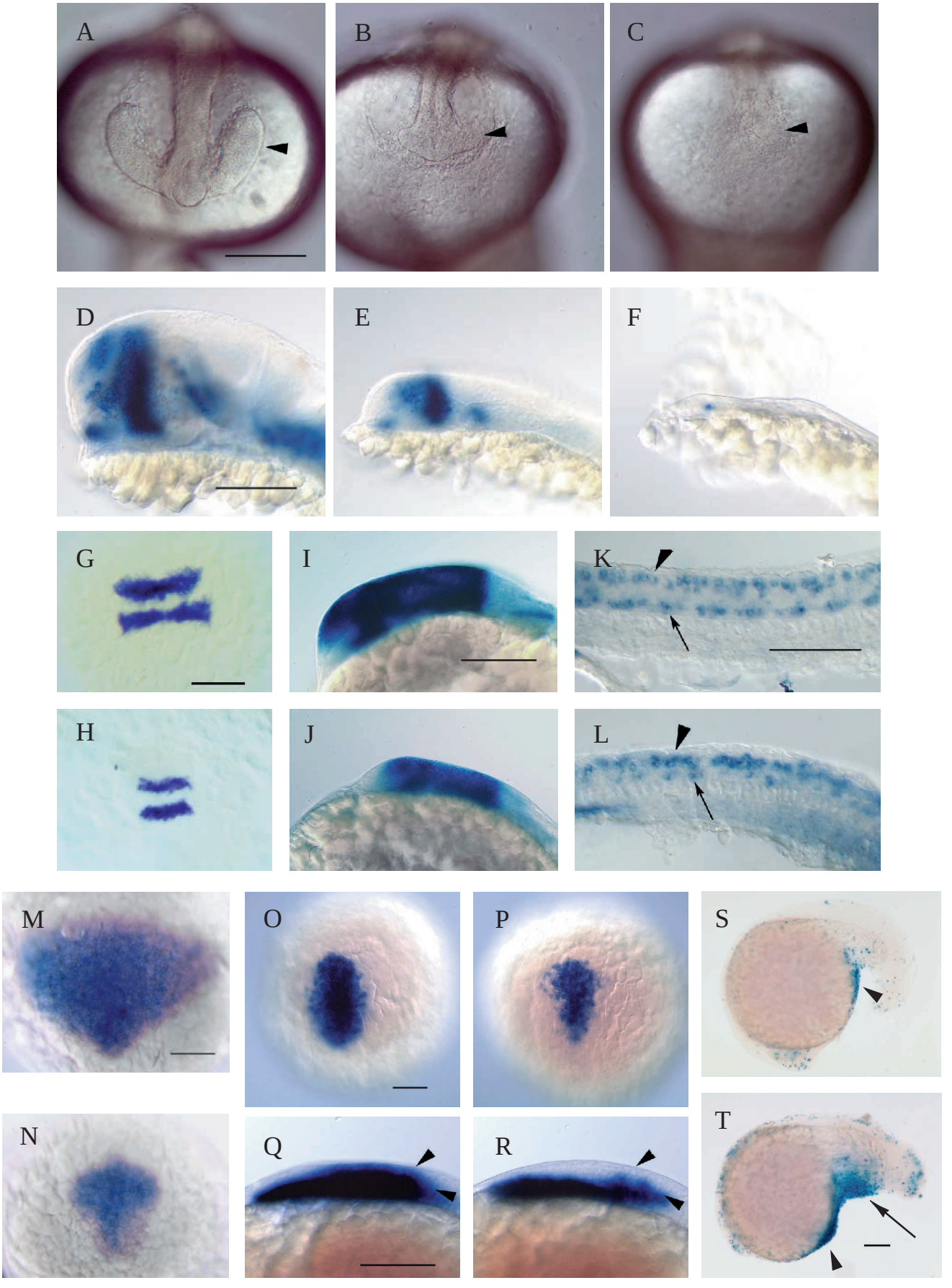
A
B
C
D
E
F
G
I
K
H
J
L
M
O
P
S
N
Q
R
T

affected, we examined expression patterns of mesodermal genes. *Hatching gland-1* (*hgg-1*) is an early marker for the hatching gland, a derivative of the prechordal plate (Thisse et al., 1994). The intensity and number of *hgg-1*-expressing cells appeared normal in *crm* mutants, although labeled cells were distributed more closely to the midline than in WT (Fig. 4A,B). Consistent with the early expression of *hgg-1*, the hatching gland appears morphologically normal at later stages (unpublished data). In the WT trunk, *α-collagen II* (*col2a1*) is expressed in floor plate, notochord, and hypochord, a row of axial cells lying just beneath the notochord (Yan et al., 1995). Expression of *col2aI* in these midline structures was essentially normal in *crm*$^{-}$ embryos (Fig. 4C,D).

In contrast to axial mesodermal derivatives, derivatives of paraxial and intermediate mesoderm were reduced in *crm* mutants. Somites are much smaller although they form at the same rate as in WT siblings (unpublished data). Accordingly, *myoD*, a marker for the myotomal component of somites (Weinberg et al., 1996), is expressed to a much lesser extent during segmentation stages (Fig. 4E,F). After gastrulation, the homeodomain gene *lim1* (Toyama et al., 1995b) is expressed in notochord and in the developing pronephric ducts derived from intermediate mesoderm (R. Toyama, personal communication). In *crm* mutants, the axial domain of *lim1* expression was largely normal, while the pronephric duct expression was dramatically reduced (Fig. 4G,H).

Blood precursor cells arise from the ventral mesoderm and eventually migrate to the site of the blood islands in the tail (Detrich et al., 1995). The transcription factor *gata2* is expressed in the blood precursors both prior to and after their migration to the blood islands (Detrich et al., 1995). In *crm*$^{-}$ embryos, an expanded pool of *gata2*-expressing cells was found in the tail (Fig. 4I,J), enabling some of the accumulated cells caudal to the anus to be identified as blood precursors. Other extra cells are probably derivatives of ventral epiblast, as the expression domain of the homeobox gene *eve1*, a marker of ventral epiblast and the developing tailbud (Joly et al., 1993), was also greatly increased in *crm* mutants (Fig. 4K,L). In summary, gene expression analyses have revealed a range of mesodermal defects in *crm* mutants, with dorsal axial mesodermal derivatives least affected, paraxial and intermediate mesoderm reduced, and ventral mesoderm increased.

Fig. 3. (A-F) CNS phenotype of *crm* alleles. Anterior nervous system of (A) WT, (B)*crm*^{b305} and (C) *crm*^{b409} diploid embryos [20 somite stage]. Note the reduced size of the optic vesicles (arrowheads) in *crm*^{b305} and their absence in *crm*^{b409} homozygotes. Expression in (D) WT, (E) *crm*^{b305} and (F) *crm*^{b409} of *lim5* [24 hours]. (A-C) Frontal views, with dorsal to the top; (D-F) side views, with anterior to the left. (G-L) Polarity is retained in *crm* mutant CNS. (G) WT and (H) *crm*^{b305} mutant *krox-20* expression at 4-6 somites. (I) WT and (J) *crm*^{b305} mutant *otx1* expression at 20 somites. (K) WT and (L) *crm*^{c4} mutant *isl1* expression in trunk spinal cord at 24 hours. Dorsal Rohon-Beard sensory neurons (arrowheads) and ventral primary motor neurons (arrows) express *isl1* (Korzh, et al., 1993; Inoue, et al., 1994). G and H are dorsal views, with anterior to the top; I-L are side views with anterior to the left. M-R: Markers of neurectoderm are reduced in *crm*$^{-}$ gastrula. (M) WT and (N) *crm*^{c4} mutant expression of *otx2* at 80% epiboly. (O, P) Expression of *gsc* [80% epiboly] in WT (O) and *crm*^{c4} mutant (P). (Q,R) Side view of *gsc* expression at same stage, in WT (Q) and mutant (R). Arrowheads delimit the ectodermal expression, which is decreased in the *crm*$^{-}$ embryo, while the underlying mesodermal expression is preserved. In M-P, view is dorsal with anterior to the top. (S,T) Increased cell death in *crm*$^{-}$ embryos. (S) WT and (T) *crm*^{c4} mutant at 18 somites, with cell death visualized in situ by terminal transferase labeling of nuclear DNA. Arrowheads indicate cluster of apoptotic cells on posterior yolk, and arrow in (T) indicates apoptotic cells in the ventral mutant tail; however, increased cell death is not found in the CNS or its precursor cells (data not shown). View is from the side, with anterior to the left. Scale bars, 100 μm.

crm^{-} embryos are ventralized at gastrulation

The overlapping *crm* deficiencies produced an invariant embryonic phenotype, differentially affecting derivatives of both mesoderm and ectoderm. Decreased cell numbers in some regions of the mutant embryo and a corresponding increase in other regions, led us to examine cell distribution at gastrulation. The zebrafish *Brachyury* homologue *no tail* (*ntl*) is expressed in mesodermal precursor cells around the margin prior to involution, after which its expression is turned off in all but axial mesoderm and the tail bud (Schulte-Merker et al., 1992). In *crm* mutants, marginal expression of *ntl* was broadened ventrally and narrowed dorsally adjacent to the developing notochord (Fig. 5A,B), suggesting that fewer mesodermal cells had converged toward the dorsal side of the embryo. The basis for this difference may be a shift in mesodermal identities. For example, early *gata2* expression in WT embryos is confined to a crescent of marginal cells at the ventral side of the gastrula (Detrich et al., 1995), thus defining ventral mesoderm. However, in *crm* mutants, the *gata2* expression domain was dramatically increased around the margin, expanded to include all but a small region encompassing the dorsal embryonic shield (Fig. 5C,D).

At the beginning of gastrulation, *eve1* is expressed in the epiblast over the ventral margin (Joly et al., 1993). In *crm* mutants, *eve1* was expressed in a greater circumference around the germ ring at early shield stage (Fig. 5E,F). For comparison, a double in situ hybridization was performed for *eve1* and for *gsc*, an early marker of the dorsal embryonic shield (Stachel et al., 1993; Schulte-Merker et al., 1994a) (Fig. 5G,H). By the late shield stage, *eve1* expression in the mutants had expanded to the edge of the *gsc* expression domain, while the extent of *gsc* expression was the same in mutant and WT (brackets). Thus, at the onset of gastrulation in *crm*$^{-}$ embryos, cells in lateral regions of the embryo have inappropriately adopted properties of more ventral cells, while dorsal axial cells appear unaffected.

DISCUSSION

Genetic analysis of *cerebum* alleles

The *cerebum* chromosomal region is an efficient target for γ-ray mutagenesis. Genetic mapping analyses demonstrate that the five γ-ray-induced *crm* alleles result from partial deletions of the distal arm of LG 15. The c4 allele segregates as a simple deficiency; however, several lines of evidence indicate that *crm*^{b305} and *crm*^{b386} are maintained as balanced reciprocal translocations. For each of these alleles, a separate mutant phenotype is found among sibling embryos from intercrosses or from haploids produced from *crm*/+ carriers, and the observed frequency of mutant classes is consistent with transmission of balanced translocations. Additionally, in the case of *crm*^{b305}, we have shown that haploids with the cosegregating mutant phenotype *ghost* have an extra copy of a DNA marker

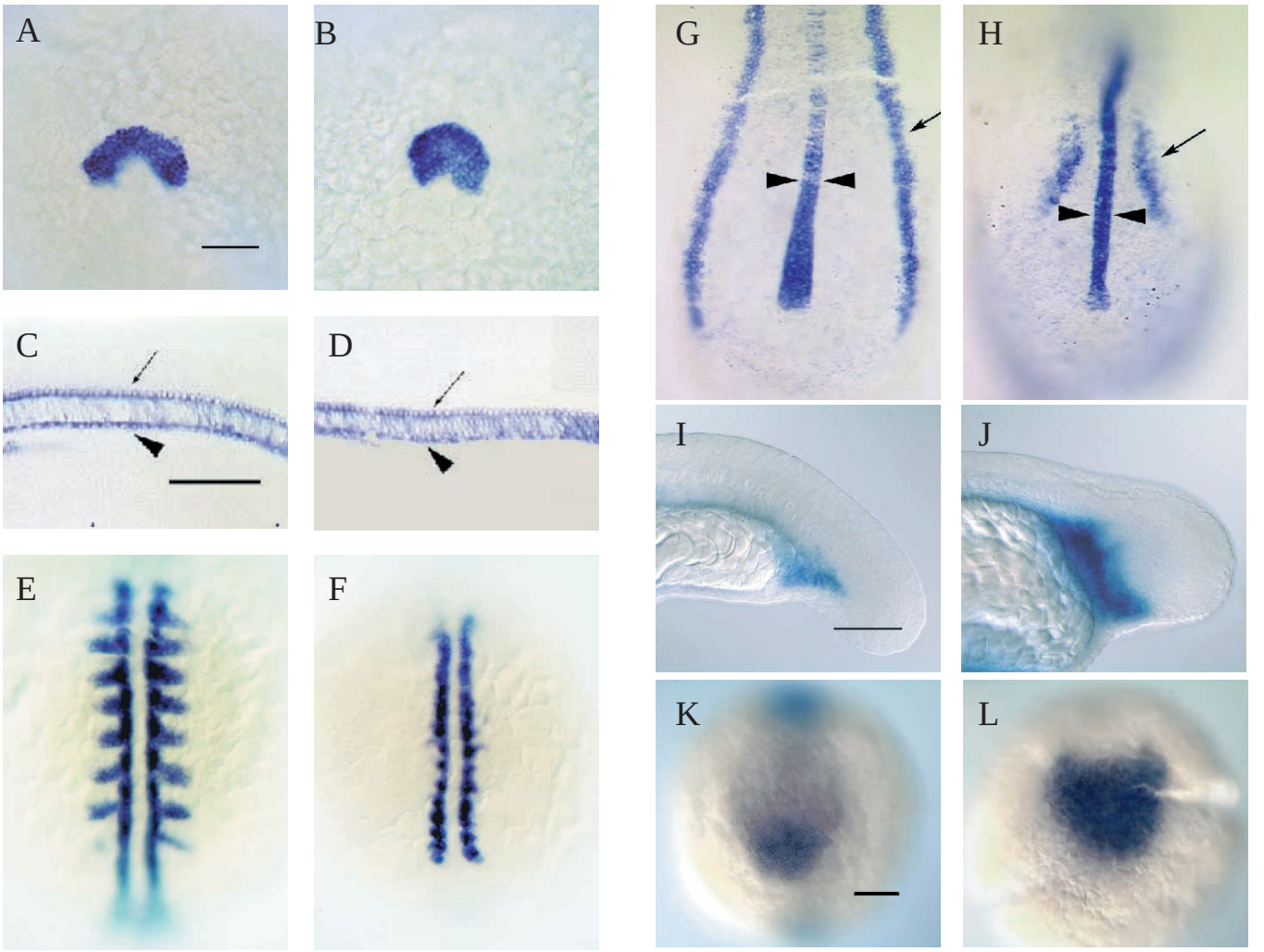

Fig. 4. Differential response of mesodermal derivatives to loss of *cerebum* activity. (A,B) Expression of *hgg-1* at the 4-6 somite stage in (A) WT and (B) *crm* mutant in presumptive hatching gland cells. (C,D) Expression of *col2a1* in the trunk of WT (C) and mutant (D) [24 hours]. In addition to the notochord, *col2a1* is expressed in the floor plate (arrows) overlying the notochord, and the hypochord (arrowheads), a row of endodermal cells beneath the notochord. (E,F) *myoD* expression [8 somite stage] in WT (E) and mutant (F). At least a subset of the *myoD*-expressing adaxial cells (Weinberg et al., 1996) are present in the mutant, consistent with the later development of muscle pioneers (S. Fisher, unpubl. obs.). (G,H) The width of the axial domain of *lim1* expression (arrowheads) in the developing notochord is similar in WT (G) and mutant (H), while expression in the developing pronephric ducts (arrows) is greatly decreased in the mutant [8 somite stage]. (I,J) The expanded pool of blood precursor cells in the *crm* mutant (J) compared to WT (I) is revealed by expression of *gata2* [20 somite stage]. (K,L) Ventral tail bud expression of *eve1* [8 somite stage] is also expanded in the mutant (L) compared to WT (K). A,B and E-H are dorsal views, with anterior to the top. C,D,I and J are side views with anterior to the left. K and L are posterior views, with dorsal to the top. Scale bars = 100 μm; E-H and L are the same magnification as K.

that is deleted in crm^{-} haploids. The lesion in crm^{b409} is more complex; the deletion of sequences in two unlinked regions, with intervening sequences intact, is suggestive of an inversion with an accompanying loss of some chromosomal material. We hypothesize that the more severe brain phenotype in crm^{b409} is due to the added deletion of *lim1*, as the absence of forebrain and midbrain in b409 homozygotes is similar to the phenotype described for *Lim1* homozygous mutants produced by targeted mutagenesis in the mouse (Shawlot and Behringer, 1995).

With the exception of b409, the overlapping *crm* deficiencies exhibit a single, recognizable early embryonic phenotype, despite the different amounts of genetic material deleted. This suggests that *crm* is the earliest zygotically acting gene within the overlapping deleted intervals. In support of this, ENU-induced alleles of *dino* have been recently recovered, which produce an early embryonic phenotype very similar to *crm* (Hammerschmidt et al., 1996a). In crosses to crm^{c4}, *dino* failed to complement in 41/146, or 28% of the progeny (M. Hammerschmidt and S. Fisher, unpublished data), suggesting that *dino* and *crm* are allelic, and supporting the hypothesis that the crm^{-} gastrulation phenotype is due to the loss of a single gene. Additional genetic analysis and the mapping of the *dino* alleles will confirm whether the same gene is responsible for the ventralized mutant phenotype. If this proves to be the case, the *cerebum* locus will be renamed *dino*.

Comparative analysis of the *crm* deficiencies has allowed us to order markers, and has limited the interval in which *crm* resides to approximately 17 cM, equivalent to approximately 9 megabases (Johnson et al., 1996). From the analysis of other

vertebrate genomes (Miklos and Rubin, 1996), we estimate that several hundred genes would map to a chromosomal region of this size. However, far fewer would result in embryonic lethality or encode transcripts expressed at the onset of gastrulation, as we expect of *crm*.

Ectodermal and mesodermal derivatives are both affected in *crm*⁻ embryos

Deficiencies of *crm* are pleiotropic, with multiple derivatives of ectoderm and mesoderm affected. The size of the mutant CNS is decreased; however, genes in the brain and spinal cord are expressed in appropriate anterior-posterior and dorsal-ventral patterns. Derivatives of paraxial and intermediate mesoderm are also decreased but, despite their reduced size, somites develop at the same rate as in WT, indicating that some aspects of mesodermal patterning are intact in *crm*⁻ embryos.

In contrast to the reduction of cells in other regions of the *crm*⁻ embryo, the tail is greatly enlarged. Aspects of the *crm*⁻ phenotype are reminiscent of zebrafish *spadetail* (*spt*) mutants, in which trunk somites fail to develop and cells accumulate abnormally in the tail (Kimmel et al., 1989). Interestingly, cells that accumulate in the tail of *spt* mutants express *eve1* (Joly et al., 1993), as was observed for some of the excess cells in the *crm* mutant tailbud, and both mutations result in cell death in caudal regions where cells inappropriately accumulate. Mutations in *spt* are thought to affect cell fate and subsequent movements at gastrulation, leading to the abnormal morphology of older embryos (Kimmel et al., 1989; Ho and Kane, 1990). We expect that altered cell fate and similar, early morphogenetic defects lead to the pleiotropic phenotype of *crm* mutants.

crm⁺ may function as an antagonist of ventralizing signals

Our analysis of *crm* mutants has revealed defects in dorsal-ventral patterning at gastrulation that could account for the later phenotypic severity and range of affected tissues. The reduced size of the CNS likely stems from a decrease in presumptive neurectoderm at gastrulation, since increased cell death is not observed in *crm* mutants until mid-segmentation, and then primarily in the tail. While we have not directly demonstrated a change in ectodermal cell fates accompanying the reduced neurectoderm, *crm*⁻ gastrulae clearly exhibit a shift in the identity of mesodermal cells. By 50% epiboly, cells in lateral regions of the *crm*⁻ gastrula margin inappropriately assume properties of more ventral cells. Later, a corresponding increase in ventral derivatives, such as blood, is observed. In contrast, axial midline structures derived from the dorsal embryonic shield, the zebrafish equivalent of the *Xenopus* organizer (Ho, 1992; Shih and Fraser, 1996) are largely unaffected in *crm* mutants.

We note a striking similarity between the phenotype of *crm*⁻ gastrulae and experimentally ventralized *Xenopus* embryos, in which a range of defects can be induced with subsets of mesodermal and ectodermal derivatives affected in concert (reviewed in Gerhart et al., 1991). A molecular basis for ven-

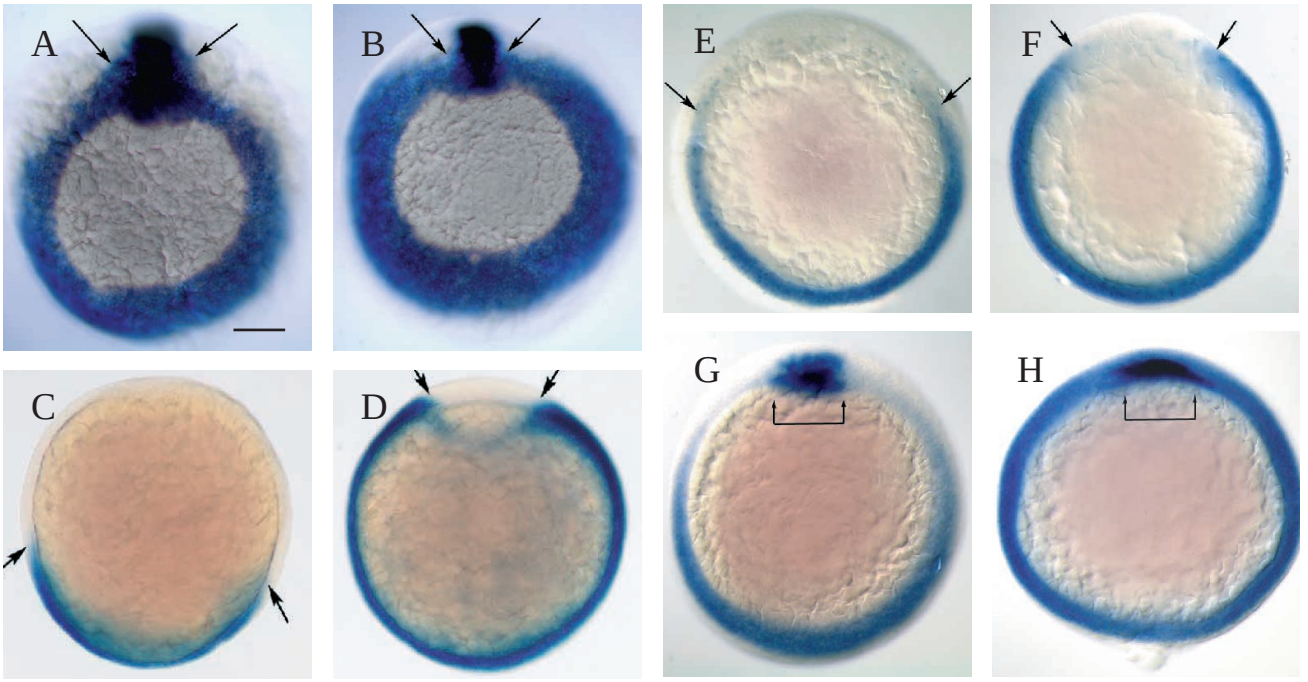

Fig. 5. Domains of ventral markers are expanded in *cerebum*⁻ gastrula. (A,B) Expression of *ntl* [80% epiboly] in WT (A) and *crm* mutant embryos (B). Mutants had fewer *ntl*-expressing cells adjacent to the dorsal axial mesoderm (arrows), and a broader domain of expression ventrally. (C,D) Expression of *gata2* [80% epiboly] (arrows) spanned an approximately 120° region on the ventral side in WT (C) but spread to an approximately 315° region of the mutant margin (D). (E,F) Expression of *eve1* in WT (E) and *crm* mutant embryos (F) at early shield stage [50% epiboly]. The expanded domain of *eve1* expression is already apparent in the *crm*⁻ embryo at early gastrulation (arrows). (G,H) Double labeling for expression of *gsc* and *eve1* in WT (G) and mutant (H) embryos at late shield stage [55% epiboly]. Although the pattern of dorsal *gsc* expression is similar in WT and mutant embryos (brackets), the expansion of *eve1* expression into the dorsolateral margin is even more apparent in the mutant at this stage. All embryos are oriented with dorsal to the top; A and B are vegetal pole views, and C-H are animal pole views. Scale bar, 100 μm.

tralization of the *Xenopus* embryo is suggested by the overexpression of BMP-4 or related signals, which can override organizer-derived dorsalizing signals (Jones et al., 1992; Fainsod et al., 1994; Clement et al., 1995; Hemmati-Brivanlou and Thomsen, 1995; Schmidt et al., 1995; Wilson and Hemmati-Brivanlou, 1995).

Evidence for the existence of ventralizing signals in the zebrafish gastrula has come from interactions between co-cultured regions in an explant system, similar to the animal cap assays widely used with *Xenopus* embryos (Sagerström et al., 1996). Loss of function of *crm* also reveals the existence of ventralizing signals in the zebrafish embryo, and further suggests that crm^+ may normally antagonize those signals. Because of the role that the organizer plays in dorsalizing the *Xenopus* embryo, and because the equivalent region appears to be spared in crm^- embryos, we propose that the *crm* locus encodes a dorsalizing factor produced by the embryonic shield, which acts to influence the fate of surrounding mesoderm and ectoderm.

Candidates for *crm* include the zebrafish homologues of genes encoding the dorsally expressed factors Noggin and Chordin. In *Xenopus* embryos, both proteins can induce dorsal mesoderm and neurectoderm and presumably act through their ability to bind BMPs with high affinity and prevent them from activating their receptors (Piccolo et al., 1996; Zimmerman et al., 1996). Furthermore, ectopic expression of a dominant negative BMP-2/4 receptor can rescue the *dino* mutant phenotype (Hammerschmidt et al., 1996b), implicating the wild-type function of this locus in regulating BMP signaling.

Using primers specific to a zebrafish *noggin* gene (Fritz et al., 1996), we have amplified the expected PCR product from DNA of the *crm* deficiency mutants, ruling out this *noggin* homologue as a candidate for *crm* (S. Fisher, unpublished data). We have isolated a partial clone of a zebrafish gene with significant homology to *Xenopus chordin* and demonstrated that it is absent from DNA of c4 and b305 homozygotes, making it a strong candidate for the *crm* gene (V. Miller and S. Fisher, unpublished data). Molecular characterization of additional mutant alleles will determine whether *crm* encodes a zebrafish *chordin* homologue.

Lack of crm^+ activity leads to an alteration in specification of the gastrula, such that an expansion of ventral epiblast and mesoderm is accompanied by a decrease in dorsolateral mesoderm and neurectoderm. Analysis of the *crm* loss-of-function phenotype has provided genetic evidence confirming the existence of ventralizing signals in the zebrafish gastrula, and has suggested a role for crm^+ as an antagonist of those signals, further demonstrating the similarity of mechanisms that underlie patterning of fish and frog embryos.

The authors gratefully acknowledge the help and hospitality of John Postlethwait and members of his laboratory in the initial experiments to map *crm* (supported by NIH grants RR/RG10715 and 1PO1HD22486). We thank Charline Walker and Chuck Kimmel, our Oregon colleagues in initial gamma mutagenesis screens (supported by NIH grant 1PO1HD22486); and Steve Johnson for providing map cross DNA, unpublished information and valuable advice on genetics. We especially thank Matthias Hammerschmidt, Reiko Toyama and Igor Dawid, Andreas Fritz, John Postlethwait and Wolfgang Driever, Eliza Shah, Mark Fishman, Howard Jacobs and Ela Knapik for sharing information prior to publication. We thank Chen-Ming Fan, Andy Fire, Amy Rubinstein, Valarie Miller and Steve Johnson for critical readings of the manuscript, and Don Brown for his helpful input. This work was supported by an NIH Clinical Investigator Development Award (NS01850-02) to S. F., and an American Cancer Society postdoctoral fellowship (PF-4087) to S. L. A.; M. E. H. is a Pew Scholar in Biomedical Research.

REFERENCES

Appel, B., Korzh, V., Glasgow, E., Thor, S., Edlund, T., Dawid, I. B. and Eisen, J. S. (1995). Motoneuron fate specification revealed by patterned LIM homeobox gene expression in embryonic zebrafish. *Development* **121**, 4117-25.

Beddington, R. S. (1994). Induction of a second neural axis by the mouse node. *Development* **120**, 613-20.

Chakrabarti, S., Streisinger, G., Singer, F. and Walker, C. (1983). Frequency of gamma-ray induced specific locus and recessive lethal mutations in mature germ cells of the zebrafish, *Brachydanio rerio*. *Genetics* **103**, 109-123.

Christian, J. L. and Moon, R. T. (1993). Interactions between Xwnt-8 and Spemann organizer signaling pathways generate dorsoventral pattern in the embryonic mesoderm of *Xenopus*. *Genes Dev.* **7**, 13-28.

Clement, J. H., Fettes, P., Knochel, S., Lef, J. and Knochel, W. (1995). Bone morphogenetic protein 2 in the early development of *Xenopus laevis*. *Mech. Dev.* **52**, 357-70.

Detrich, H. W. r., Kieran, M. W., Chan, F. Y., Barone, L. M., Yee, K., Rundstadler, J. A., Pratt, S., Ransom, D. and Zon, L. I. (1995). Intraembryonic hematopoietic cell migration during vertebrate development. *Proc. Natl Acad. Sci. USA* **92,** 10713-10717.

Fainsod, A., Steinbeisser, H. and De Robertis, E. M. (1994). On the function of BMP-4 in patterning the marginal zone of the *Xenopus* embryo. *EMBO J.* **13**, 5015-25.

Fritz, A., Rozowski, M., Walker, C. and Westerfield, M. (1996). Identification of selected gamma-ray induced deficiencies in zebrafish using multiplex polymerase chain reaction. *Genetics* **144**, 1735-1745.

Gawantka, V., Delius, H., Hirschfeld, K., Blumenstock, C. and Niehrs, C. (1995). Antagonizing the Spemann organizer: role of the homeobox gene *Xvent-1*. *EMBO J.* **14**, 6268-79.

Gerhart, J., Doniach, T. and Stewart, R. (1991). Organizing the *Xenopus* organizer. *Gastrulation* 57-77.

Graff, J. M., Thies, R. S., Song, J. J., Celeste, A. J. and Melton, D. A. (1994). Studies with a *Xenopus* BMP receptor suggest that ventral mesoderm-inducing signals override dorsal signals in vivo. *Cell* **79**, 169-79.

Halpern, M. E., Ho, R. K., Walker, C. and Kimmel, C. B. (1993). Induction of muscle pioneers and floor plate is distinguished by the zebrafish *no tail* mutation. *Cell* **75**, 99-111.

Hammerschmidt, M., Pelegri, F., Mullins, M. C., Kane, D. A., van Eeden, F. J. M., Furutani-Seiki, M., Haffter, P., Heisenberg, C.-P., Jiang, Y.-J., Kelsh, R. N., Odenthal, J., Warga, R. M. and Nüsslein-Volhard, C. (1996a). *dino* and *mercedes*, two genes regulating dorsal development in the zebrafish embryo. *Development* **123,** 95-102.

Hammerschmidt, M., Serbedzija, G. and McMahon, A. P. (1996b). Genetic analysis of dorsoventral pattern formation in the zebrafish: requirement of a Bmp4-like ventralizing activity and its dorsal repressor. *Genes Dev.* **10**, 2452-2461.

Hawley, S. H., Wunnenberg-Stapleton, K., Hashimoto, C., Laurent, M. N., Watabe, T., Blumberg, B. W. and Cho, K. W. (1995). Disruption of BMP signals in embryonic *Xenopus* ectoderm leads to direct neural induction. *Genes Dev.* **9**, 2923-35.

Hemmati-Brivanlou, A. and Thomsen, G. H. (1995). Ventral mesodermal patterning in *Xenopus* embryos: expression patterns and activities of BMP-2 and BMP-4. *Dev. Genet.* **17**, 78-89.

Ho, R. K. (1992). Axis formation in the embryo of the zebrafish, *Brachydanio rerio*. *Sem. Dev. Biol.* **3**, 53-64.

Ho, R. K. and Kane, D. A. (1990). Cell-autonomous action of zebrafish *spt-1* mutation in specific mesodermal precursors. *Nature* **348**, 728-30.

Holley, S. A., Neul, J. L., Attisano, L., Wrana, J. L., Sasai, Y., O'Connor, M. B., De Robertis, E. M. and Ferguson, E. L. (1996). The *Xenopus* dorsalizing factor noggin ventralizes Drosophila embryos by preventing DPP from activating its receptor. *Cell* **86**, 607-617.

Inoue, A., Takahashi, M., Hatta, K., Hotta, Y. and Okamoto, H. (1994). Developmental regulation of *islet-1* mRNA expression during neuronal differentiation in embryonic zebrafish. *Dev. Dynamics* **199**, 1-11.

Johnson, S. L., Gates, M. A., Johnson, M., Talbot, W. S., Horne, S., Baik, K., Rude, S., Wong, J. R. and Postlethwait, J. H. (1996). Centromere-linkage analysis and consolidation of the zebrafish genetic map. *Genetics* **142**, 1277-1288.

Joly, J. S., Joly, C., Schulte-Merker, S., Boulekbache, H. and Condamine, H. (1993). The ventral and posterior expression of the zebrafish homeobox gene *eve1* is perturbed in dorsalized and mutant embryos. *Development* **119**, 1261-75.

Jones, C. M., Lyons, K. M., Lapan, P. M., Wright, C. V. and Hogan, B. L. (1992). DVR-4 (bone morphogenetic protein-4) as a posterior-ventralizing factor in *Xenopus* mesoderm induction. *Development* **115**, 639-47.

Kimmel, C. B. (1989). Genetics and early development of zebrafish. *Trends Genet.* **5**, 283-8.

Kimmel, C. B., Ballard, W. W., Kimmel, S. R., Ullmann, B. and Schilling, T. F. (1995). Stages of embryonic development of the zebrafish. *Dev. Dynamics* **203**, 253-310.

Kimmel, C. B., Kane, D. A., Walker, C., Warga, R. M. and Rothman, M. B. (1989). A mutation that changes cell movement and cell fate in the zebrafish embryo. *Nature* **337**, 358-62.

Kintner, C. R. and Dodd, J. (1991). Hensen's node induces neural tissue in *Xenopus* ectoderm. Implications for the action of the organizer in neural induction. *Development* **113**, 1495-505.

Knapik, E. W., Goodman, A., Atkinson, O. S., Roberts, C. T., Shiozawa, M., Sim, C. U., Weksler-Zangen, S., Trolliet, M. R., Futrell, C., Innes, B. A., Koike, G., McLaughlin, M. G., Pierre, L., Simon, J. S., Vilallonga, E., Roy, M., Chiang, P.-W., Fishman, M. C., Driever, W. and Jacob, H. J. (1996). A reference cross DNA panel for zebrafish (*Danio rerio*) anchored with simple sequence length polymorphisms. *Development* **123,** 451-460.

Korzh, V., Edlund, T. and Thor, S. (1993). Zebrafish primary neurons initiate expression of the LIM homeodomain protein Isl-1 at the end of gastrulation. *Development* **118**, 417-25.

Ladher, R., Mohun, T. J., Smith, J. C. and Snape, A. M. (1996). *Xom*: a *Xenopus* homeobox gene that mediates the early effects of BMP-4. *Development* **122**, 2385-2394.

Li, Y., Allende, M. L., Finkelstein, R. and Weinberg, E. S. (1994). Expression of two zebrafish *orthodenticle*-related genes in the embryonic brain. *Mech. Dev.* **48**, 229-44.

Miklos, G. L. G. and Rubin, G. M. (1996). The role of the genome project in determining gene function: insights from model organisms. *Cell* **86**, 521-529.

Mullins, M. C., Hammerschmidt, M., Haffter, P. and Nüsslein-Volhard, C. (1994). Large-scale mutagenesis in the zebrafish: in search of genes controlling development in a vertebrate. *Curr. Biol.* **4**, 189-202.

Oxtoby, E. and Jowett, T. (1993). Cloning of the zebrafish *krox-20* gene (*krx-20*) and its expression during hindbrain development. *Nucleic Acids Res.* **21**, 1087-95.

Piccolo, S., Sasai, Y., Lu, B. and De Robertis, E. M. (1996). Dorsoventral patterning in Xenopus: Inhibition of ventral signals by direct binding of chordin to BMP-4. *Cell* **86**, 589-598.

Postlethwait, J. H., Johnson, S. L., Midson, C. N., Talbot, W. S., Gates, M., Ballinger, E. W., Africa, D., Andrews, R., Carl, T., Eisen, J. S., Horne, S., Kimmel, C. B., Hutchinson, M., Johnson, M. and Rodriguez, A. (1994). A genetic linkage map for the zebrafish. *Science* **264**, 699-703.

Sagerström, C. G., Grinblat, Y. and Sive, H. (1996). Anteroposterior patterning in the zebrafish, *Danio rerio*: an explant assay reveals inductive and suppressive interactions. *Development* **122**, 1873-1883.

Sasai, Y., Lu, B., Steinbeisser, H., Geissert, D., Gont, L. K. and De Robertis, E. M. (1994). *Xenopus* chordin: a novel dorsalizing factor activated by organizer-specific homeobox genes. *Cell* **79**, 779-90.

Schmidt, J. E., Suzuki, A., Ueno, N. and Kimelman, D. (1995). Localized BMP-4 mediates dorsal/ventral patterning in the early *Xenopus* embryo. *Dev. Biol.* **169**, 37-50.

Schmidt, J. E., von Dassow, G. and Kimelman, D. (1996). Regulation of dorsal-ventral patterning: the ventralizing effects of the novel *Xenopus* homeobox gene *Vox*. *Development* **122**, 1711-1721.

Schulte-Merker, S., Hammerschmidt, M., Beuchle, D., Cho, K. W., De Robertis, E. M. and Nüsslein-Volhard, C. (1994a). Expression of zebrafish *goosecoid* and *no tail* gene products in wild-type and mutant *no tail* embryos. *Development* **120**, 843-52.

Schulte-Merker, S., Ho, R. K., Herrmann, B. G. and Nusslein-Volhard, C. (1992). The protein product of the zebrafish homologue of the mouse *T* gene is expressed in nuclei of the germ ring and the notochord of the early embryo. *Development* **116**, 1021-32.

Schulte-Merker, S., van Eeden, F. J., Halpern, M. E., Kimmel, C. B. and Nüsslein-Volhard, C. (1994b). *no tail* (*ntl*) is the zebrafish homologue of the mouse *T* (*Brachyury*) gene. *Development* **120**, 1009-15.

Shawlot, W. and Behringer, R. R. (1995). Requirement for *Lim1* in head-organizer function. *Nature* **374**, 425-30.

Shih, J. and Fraser, S. E. (1996). Characterizing the zebrafish organizer: microsurgical analysis at the early-shield stage. *Development* **122**, 1313-22.

Sive, H. L. (1993). The frog prince-ss: a molecular formula for dorsoventral patterning in *Xenopus*. *Genes Dev.* **7**, 1-12.

Slack, J. M. (1994). Inducing factors in *Xenopus* early embryos. *Curr. Biol.* **4**, 116-26.

Smith, W. C., and Harland, R. M. (1992). Expression cloning of *noggin*, a new dorsalizing factor localized to the Spemann organizer in *Xenopus* embryos. *Cell* **70**, 829-840.

Solnica-Krezel, L., Schier, A. F. and Driever, W. (1994). Efficient recovery of ENU-induced mutations from the zebrafish germline. *Genetics* **136**, 1401-20.

Spemann, H. and Mangold, H. (1924). Über induktion von Embryonalanlagen dürch Implantation artfremder Organisatoren. *Roux's Arch. EntwMech. Org.* **100**, 599-638.

Stachel, S. E., Grunwald, D. J. and Myers, P. Z. (1993). Lithium perturbation and goosecoid expression identify a dorsal specification pathway in the pregastrula zebrafish. *Development* **117**, 1261-74.

Steinbeisser, H., Fainsod, A., Niehrs, C., Sasai, Y. and De Robertis, E. M. (1995). The role of *gsc* and BMP-4 in dorsal-ventral patterning of the marginal zone in *Xenopus*: a loss-of-function study using antisense RNA. *EMBO J* **14**, 5230-43.

Stewart, R. M. and Gerhart, J. C. (1990). The anterior extent of dorsal development of the *Xenopus* embryonic axis depends on the quantity of organizer in the late blastula. *Development* **109**, 363-72.

Storey, K., Crossley, J. M., De Robertis, E., Norris, W. E. and Stern, C. D. (1992). Neural induction and regionalisation in the chick embryo. *Development* **114**, 729-741.

Striesinger, G., Walker, C., Dower, N., Knauber, D., and Singer, F. (1981). Production of clones of homozygous diploid zebrafish (*Brachydanio rerio*). *Nature* **291**, 293-296.

Talbot, W. S., Trevarrow, B., Halpern, M. E., Melby, A. E., Farr, G., Postlethwait, J. H., Jowett, T., Kimmel, C. B. and Kimelman, D. (1995). A homeobox gene essential for zebrafish notochord development. *Nature* **378**, 150-7.

Thisse, C., Thisse, B., Halpern, M. E. and Postlethwait, J. H. (1994). Goosecoid expression in neurectoderm and mesendoderm is disrupted in zebrafish *cyclops* gastrulas. *Dev. Biol.* **164**, 420-9.

Thisse, C., Thisse, B., Schilling, T. F. and Postlethwait, J. H. (1993). Structure of the zebrafish *snail1* gene and its expression in wild-type, *spadetail* and *no tail* mutant embryos. *Development* **119**, 1203-15.

Thor, S., Ericson, J., Brannstrom, T., and Edlund, T. (1991). The homeodomain LIM protein Isl-1 is expressed in subsets of neurons and endocrine cells in the adult rat. *Neuron* **7**, 881-889.

Toyama, R., Curtiss, P. E., Otani, H., Kimura, M., Dawid, I. B. and Taira, M. (1995a). The LIM class homeobox gene *lim5*: implied role in CNS patterning in *Xenopus* and zebrafish. *Dev. Biol.* **170**, 583-93.

Toyama, R., O'Connell, M. L., Wright, C. V., Kuehn, M. R. and Dawid, I. B. (1995b). *Nodal* induces ectopic goosecoid and *lim1* expression and axis duplication in zebrafish. *Development* **121**, 383-91.

Weinberg, E. S., Allende, M. L., Kelly, C. S., Abdelhamid, A., Murakami, T., Andermann, P., Doerre, O. G., Grunwald, D. J. and Riggleman, B. (1996). Developmental regulation of zebrafish *MyoD* in wild-type, *no tail* and *spadetail* embryos. *Development* **122**, 271-80.

Westerfield, M. (ed.) (1993). *The Zebrafish Book*. Eugene, OR: University of Oregon Press.

Wilson, P. A. and Hemmati-Brivanlou, A. (1995). Induction of epidermis and inhibition of neural fate by Bmp-4. *Nature* **376**, 331-3.

Winnier, G., Blessing, M., Labosky, P. A. and Hogan, B. L. (1995). *Bone morphogenetic protein-4* is required for mesoderm formation and patterning in the mouse. *Genes Dev.* **9**, 2105-16.

Yan, Y. L., Hatta, K., Riggleman, B. and Postlethwait, J. H. (1995). Expression of a type II collagen gene in the zebrafish embryonic axis. *Dev. Dynamics* **203**, 363-76.

Zimmerman, L. B., De Jesús-Escobar, J. and Harland, R. M. (1996). The Spemann organizer signal noggin binds and inactivates bone morphogenetic protein 4. *Cell* **86**, 599-606.

(Accepted 27 January 1997)